PASJ: Publ. Astron. Soc. Japan **62**, 431–439, 2010 April 25

Japanese VLBI Network Mapping of SiO $v = 3$ $J = 1$–0 Maser Emission in W Hydrae

Hiroshi IMAI,[1] Jun-ichi NAKASHIMA,[2] Shuji DEGUCHI,[3] Aya YAMAUCHI,[4]
Akiharu NAKAGAWA,[1] and Takumi NAGAYAMA[1]
[1]*Graduate School of Science and Engineering, Kagoshima University, 1-21-35 Korimoto, Kagoshima, Kagoshima 890-0065*
hiroimai@sci.kagoshima-u.ac.jp
[2]*Department of Physics, University of Hong Kong, Pokfulam Road, Hong Kong, China*
[3]*Nobeyama Radio Observatory, National Astronomical Observatory of Japan, Minamimaki, Minamisaku, Nagano 384-1305*
[4]*Mizusawa VLBI Observatory, National Astronomical Observatory of Japan, 2-21-1 Osawa, Mitaka, Tokyo 181-8588*

(Received 2009 November 24; accepted 2010 February 1)

Abstract

We report first on two-epoch mapping observations of SiO $v = 3$ $J = 1$–0 maser emission in the semiregular variable W Hydrae using the Japanese VLBI Network. The flux density of the $v = 3$ $J = 1$–0 emission detected on 2009 February 28 was two orders of magnitude smaller than those of the $v = 1$ and $v = 2$ emissions, while a month and half later the $v = 3$ flux density suddenly increased by a factor of $\sim$25. In contrast, the $v = 1$ and $v = 2$ flux densities decreased during this period, as expected from the optical light curve. At the first epoch, the $v = 3$ maser features were located inside of a ring composed of the $v = 1$ and $v = 2$ features by 6 mas ($\gtrsim$0.5 AU) toward the central star. These offsets are meaningfully larger than the error of the fitted ring radius and the difference in the ring sizes of $v = 1$ and $v = 2$ masers ($\lesssim$0.2 AU). The present result at the first epoch suggests that $v = 3$ $J = 1$–0 SiO masers are predominantly excited in a pumping mechanism (e.g., collisional pumping) different from that recently proposed on the basis of the line overlap with infrared H_2O lines. Interestingly, the second-epoch observation revealed that the $v = 3$ features were located on almost the same ring as the $v = 2$ ring, which is consistent with what line-overlap theory suggests.

Key words: masers — stars: AGB and post-AGB — stars: individual (W Hydrae)

1. Introduction

Silicon monoxide (SiO) maser emission is a useful probe for elucidating the dynamics of mass-loss outflows from asymptotic giant branch (AGB) and post-AGB stars, some of which exhibit stellar pulsation (e.g., Mira variables). SiO maser emission usually exhibits a ring-like distribution with a typical radius of 2–3 stellar radii of the central star. Multi-epoch very long baseline interferometric (VLBI) observations have found that the dynamical expansion and contraction of the circumstellar envelopes (CSEs) are actually reflected by the feature motions (e.g., Diamond & Kemball 2003), though some attention should be paid to the physical interpretation on the line-of-sight velocity distribution and the proper motions of the maser features (tiny gas clumps) (e.g., Matsumoto et al. 2008). In practice, it is difficult to trace the temporal variation of the physical conditions in the SiO maser regions because it is impossible to directly estimate the physical parameters in the maser regions in CSEs to date.

A problem in studying SiO masers is the maser excitation mechanism. It should give direct estimations of the densities and temperatures of maser clumps in the envelope, if properly modeled. Several maser transitions are observed at the same time in a maser source. A statistical analysis of the single-dish observation data of the three SiO $J = 1$–0 masers at different vibrational levels showed a clear correlation between the maser intensity ratios and the infrared color of the star (Nakashima & Deguchi 2007), suggesting that the radiative pumping schemes of maser excitation are predominant. The energy spacing between the adjacent vibrational levels of the SiO molecule is as large as 1780 K in temperature scale. Interestingly, VLBI observations have revealed that both $v = 1$ and $v = 2$ masers are found to come from almost the same region (within 1 AU), and that they have nearly equal luminosities (e.g., Miyoshi et al. 1994; Desmurs et al. 2000; Yi et al. 2005). Soria-Ruiz et al. (2004) demonstrated for the first time that the difference in the spatial distributions of the $(v = 1)/(v = 2)$ $J = 1$–0 and $v = 1$ $J = 2$–1 maser lines depends on the stellar type (S- or O-rich), suggesting that a radiative pumping scheme including the line-overlap between H_2O and SiO vibrational transitions should be taken into account for maser excitation at a higher vibrational level. However, the pumping mechanism for the $v = 3$ masers remains unclear due to a lack of information on its spatial distribution. Differences in the spatial distributions of the $J = 1$–0 masers at $v = 1$ and $v = 2$ have been investigated in detail; the difference, especially in the radii of rings in the emission distributions, is small (<1 AU), seeming to lead to the conclusion of predominance of the line-overlap mechanism rather than collisional pumping schemes (e.g., Lockett & Elitzur 1992; Humphreys et al. 2002). However, the latter schemes also reproduce the distributions of the $v = 1$ and $v = 2$ masers, matching the predictions of the former schemes. Since the radiative and collisional pumping schemes predict significantly different tendencies of the spatial distribution of the

Table 1. Parameters of the JVN observations.

Code* (rYYDDDx)	Duration [UT]	Maser line	Telescopes†	$V_{\rm LSR}$‡ [km s^{-1}]	1-σ noise [Jy beam^{-1}]	Synthesized beam§	Notes‖
r09058a	15:30–21:10	$v = 1$	MROS	41.4	0.13	$0.84 \times 0.51, -28.5$	1
		$v = 2$		...	0.12	$0.86 \times 0.51, -23.9$	1, 2, 3
r09059b	15:35–21:10	$v = 2$	MROS	43.9	0.07	$1.35 \times 0.60, -13.4$	4
		$v = 3$		...	0.02	$1.21 \times 0.60, \ -8.4$	4, 5
r09101a	12:15–18:00	$v = 2$	MRSNK	...	...	...	6, 7, 8
		$v = 3$		...	...	...	5, 6, 7, 8
r09102a	12:00–17:51	$v = 2$	MROSNK	40.3	0.05	$3.41 \times 0.64, -24.8$	9, 10
		$v = 3$		40.3	0.04	$2.43 \times 0.73, -21.9$	5, 9, 10

* Observation code in JVN. YY, DDD, and x (=a, b, ...) show the year, the day of the year at the observation, and the numbering of the observations in the same date, respectively.

† Telescopes providing valid visibility data. M: VERA telescope at Mizusawa station, R: Iriki, O: Ogasawara, S: Ishigakijima, K: the NICT 34 m telescope at Kashima, N: the NRO 45 m telescope.

‡ LSR velocity of the fringe phase- and position-reference channels in data calibration.

§ Beam size, in units of mas, and position angle, in units of degree, of the synthesized beam.

‖ 1: Heavy rain at Ishigaki in the whole observation, $T_{\rm sys} > 1200$ K, 2: Missing data from Iriki due to unknown reasons, 3: Phase-referenced to the $v = 1$ data in the same code observation, 4: Heavy rain at Iriki in the first two hours, $T_{\rm sys} > 1000$ K, 5: Phase-referenced to the $v = 2$ data in the same code observation. 6: Valid data from the NRO 45 m telescope for only last one hour, 7: All data were merged with those of r09102a, 8: The NRO 45 m telescope participated in the observation during 12:19–17:26. 9: The NRO 45 m telescope participated in the observation during 12:20–17:21, 10: Valid data from the VERA Ogasawara telescope for only last two hours.

maser emission at $v = 3$ with respect to those at $v = 1$ and 2 emissions (Lockett & Elitzur 1992), VLBI observations of the $v = 3$ maser emission will provide stronger constraints on the possible pumping mechanism or the contribution fractions from the two schemes. Unfortunately, there are a limited number of sources with $v = 3$ maser emission bright enough (>1 Jy) to make a VLBI map with the current VLBI sensitivity (Cho et al. 1996; Nakashima & Deguchi 2007).

Here, we report success for the first time in VLBI mapping of the $v = 3$ maser emission, which was made toward the semi-regular (SRa) variable star W Hya. The distance to W Hya is adopted to be 80 pc in the present paper, which was derived from the revised Hipparcos catalog (Knapp et al. 2003; cf. $\sim$100 pc determined from an annual parallax measurement by Vlemmings et al. 2003). Previous VLBI observations using the Kashima–Nobeyama Interferometer (KNIFE) revealed good spatial coincidence of SiO $v = 1$ and $v = 2$ $J = 1$–0 masers in W Hya within 0.6 AU ($\sim$7 mas), even with its short (200 km) baseline (Miyoshi et al. 1994). Because W Hya is one of the brightest SiO maser sources emitting the $v = 3$ maser (Cho et al. 1996), and it is close to the Sun, it is the best target for the present SiO maser study. It is relatively easy to identify a small difference in the morphologies of the $v = 1$, 2, and 3 masers. In the present paper, we report on Japanese VLBI Network (JVN) observations of the W Hya SiO masers with higher angular resolution and higher sensitivity than those previously conducted using KNIFE. We found clear differences in the maser distribution of the $v = 3$ emission from those of the $v = 1$ and 2 emissions. A possible pumping mechanism is discussed based on the present VLBI observations.

2. Observations and Data Reduction

We simultaneously observed two pairs of SiO maser lines ($v = 1/v = 2$ and $v = 2/v = 3$ $J = 1$–0) in W Hya on 2009 February 27–28 (codes r09058a and r09059b) and April 11–12 (r09101a and r09102a) using six telescopes of the JVN: the four 20 m telescopes of the VLBI Exploration of Radio Astrometry (VERA);[1] the 45 m telescope of Nobeyama Radio Observatory (NRO);[1] and the 34 m telescope of the National Institute of Communications Technology (NICT). Table 1 gives some parameters of the observations and data reduction.

In each epoch, the observation was made for $\sim$6 hr, including scans of calibrators (NRAO 530 and J134215.3−290042). In the present paper, $\nu = 43.122079$ GHz, 42.820582 GHz, and 42.519340 GHz are adopted as rest frequencies for the SiO $v = 1$, 2, and 3 ($J = 1$–0) transitions, respectively. The system temperatures were 250–300 K in the VERA telescopes, 450–500 K in the NICT 34 m telescope, and 200–250 K in the NRO 45 m telescope. The observed signals, received in left-hand circular polarization, were digitized in four levels, divided into two base band channels each with a band width of 16 MHz (covering $\sim$111 km s^{-1} in velocity), and recorded with the SONY DIR1000 recorder at a rate of 128 Mbits s^{-1}. Thus, only two of the three maser transitions, whose rest frequencies are split within 512 MHz, could be observed at the same time. In 2009 February, the $v = 1$ and $v = 2$ transitions were observed in the code r09058a and the $v = 2$ and $v = 3$ transitions were observed the next day. In observations in 2009 April (r09101a and r09102a), only the $v = 2$ and $v = 3$ pair was observed. Because the $v = 3$ and $v = 2$ data were obtained for only one hour from the NRO 45 m telescope in r09101a, the all data in r09102a were merged with those in r09102a in order to obtain single-epoch $v = 2$ and $v = 3$ maser maps. Instead, an observation of the $v = 1$ and $v = 2$ pair was replaced by that of the $v = 2$ and $v = 3$ pair in r09102a. A data correlation was made with the Mitaka FX correlator. The accumulation period of the correlation was set to 1 s. The

[1] The NRO and VERA/Mizusawa VLBI observatories are branches of the National Astronomical Observatory, an interuniversity research institute operated by the Ministry of Education, Culture, Sports, Science and Technology.

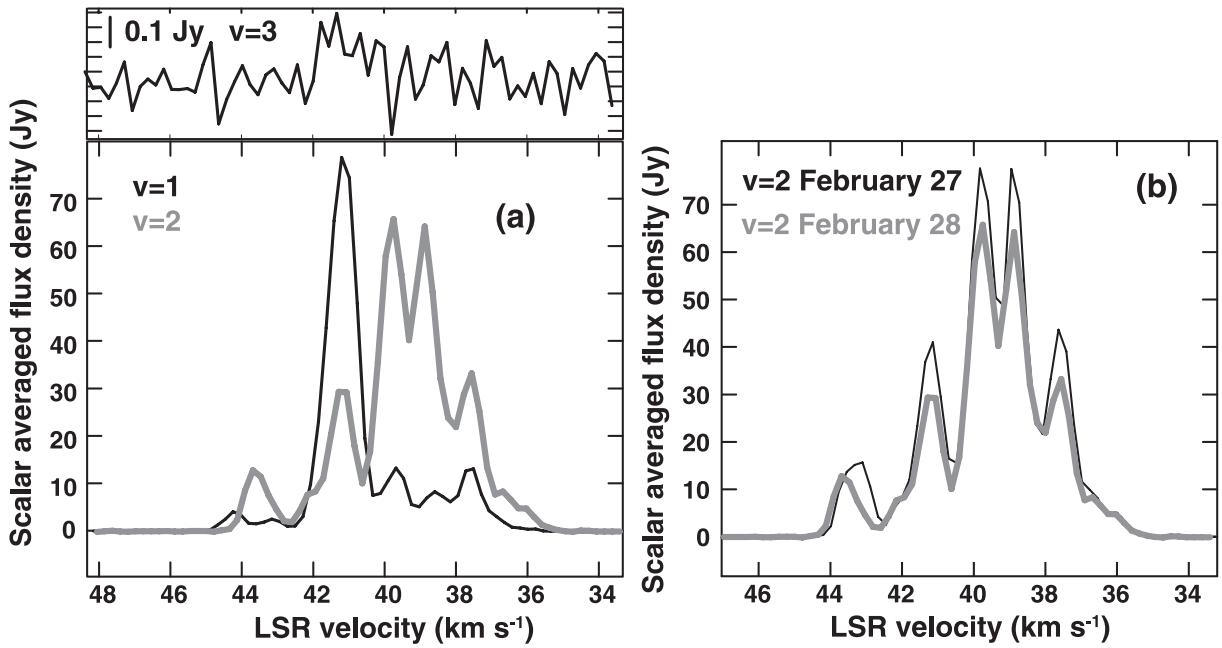

Fig. 1. Scalar-averaged cross-power spectra of SiO $v = 1$, 2, and 3 $J = 1$–0 maser emission in W Hya observed on 2009 February 27–28. The spectra were obtained by integrating data from all baselines for the whole observation time. A zero-level baseline was already subtracted from the original spectrum. (a) Spectra of the $v = 1$, 2, and 3 maser emissions. (b) Comparison between the $v = 2$ spectra observed on February 27 and 28.

coordinates of W Hya [RA (J2000.0) = $13^{\rm h}49^{\rm m}01.^{\rm s}9636$, Dec (J2000.0) = $-28°22'04.''039$] around the observation epochs were estimated from extrapolation of the astrometric parameters determined in the revised Hipparcos catalog (Knapp et al. 2003) and used for delay-tracking. The correlation outputs consisted of 512 velocity channels, yielding a velocity spacing of 0.22 km s^{-1} each.

In order to obtain image cubes for the maser source, data reduction was made using the NRAO AIPS package. First of all, visibility amplitude calibration was made using system noise temperatures and antenna gains. The bandpass amplitude characteristics were measured and corrected using scans of continuum calibrators. An instrumental group-delay calibration using the calibrator data and a Doppler-shift correction for the maser source visibilities were made. Then, fringe fitting and self-calibration were performed using visibilities in a Doppler-velocity channel shown in column 5 of table 1, which includes a bright maser spot (velocity component). The Doppler velocities are given with respect to the local standard of rest (LSR). The solutions were applied to data in other velocity channels. Typical sizes of the synthesized beams were 0.5 and 1 milliarcsecond (mas) in the observations in 2009 February and April, respectively.

Note that the data of the maser transitions with weaker flux densities were calibrated with those of the brighter maser transition in the same code observation (see the last column in table 1). For instance, in r09059b, in order to obtain the $v = 3$ maser image cube, the visibilities in the velocity channel at $V_{\rm LSR} = 43.9$ km s^{-1} in the $v = 2$ transition were calibrated in the fringe-fitting and self-calibration, whose solutions were applied to all visibilities in all of the spectral channels of the $v = 3$ as well as $v = 2$ transitions. Then, the maser distributions of two transitions were directly measured with respect to the phase-reference maser spot in one of the two transitions. The uncertainty of the positional comparison between two transitions, σ_θ, was estimated using

$$\sigma_\theta \sim \frac{\Delta\nu}{\nu}\left(\Delta\theta + \frac{c\sigma_{\tau_{\rm g}}}{D}\right), \quad (1)$$

where $\Delta\nu \simeq 300$ MHz is the rest frequency separation of the two transitions, $\Delta\theta < 50$ mas the position offset of the phase-reference maser spot with respect to the delay-tracking center, $\sigma_{\tau_{\rm g}} < 5$ ns the residual group delay, D the baseline length (typically $D \sim 1000$ km for JVN), and c the speed of light, respectively. The large position offset of the phase-reference maser spot roughly corresponds to the angular distance to the spot ($\Delta\theta \lesssim 40$ mas) from the star center, whose coordinates may have an uncertainty of within ~ 10 mas. The resulting uncertainty was estimated to be smaller than 1.5 mas (0.7 mas and 2.2 mas from the first and second terms of the right side, respectively). Thus, the uncertainty of the positional comparison is dominated by the accuracy of the group-delay residual determination using the calibrator data. This is separately described in Appendix. In conclusion, we estimated the positional comparison uncertainty within 2.3 mas. For clarity, as will be mentioned in section 3, the $v = 1$ and $v = 3$ emission images obtained through the fringe-fitting and the self-calibration using their own visibilities (valid for the $v = 3$ emission only in r09101a–r09102a) were registered onto the $v = 2$ emission image using position reference maser spots in $v = 1$ and $v = 3$ emissions, whose position was measured on the $v = 2$ emission image.

3. Results

Figure 1a shows the scalar-averaged cross power spectra of

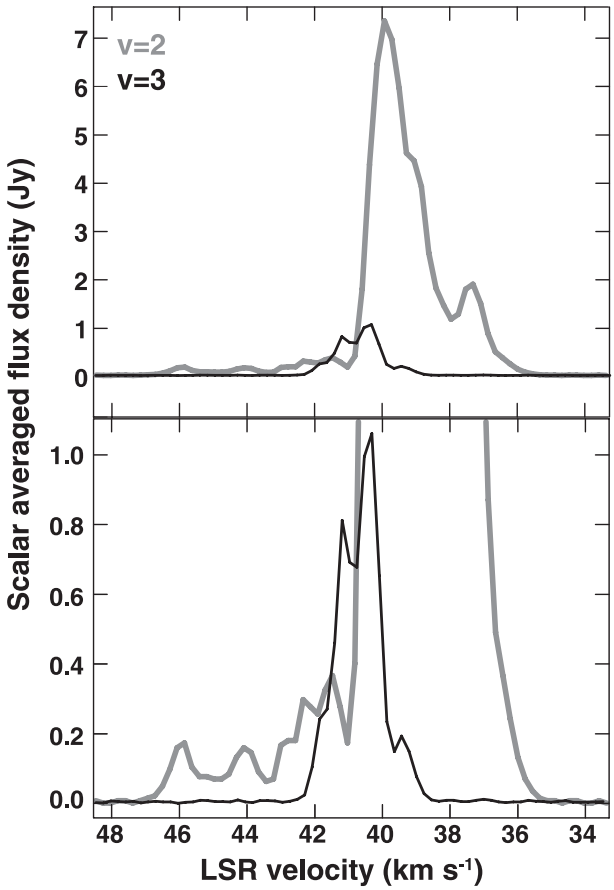

Fig. 2. Same as figure 1, but for the SiO $v = 2$ and 3 $J = 1$–0 maser emission observed on 2009 April 12. The upper and lower panels display the whole spectra and the zoom-up along the flux density for the spectra, respectively.

the three maser lines on 2009 February 27–28. Although the $v = 3$ line had a flux density comparable to those of the $v = 1$ and $v = 2$ lines in previous observations (Cho et al. 1996), it was weaker by two orders of magnitude in the present observation. The $v = 3$ emission could not be detected to an upper limit of 0.4 Jy (3-σ noise level) in the total-power spectrum, which had noise higher than that in the cross-power spectrum obtained by integrating all baseline data. It had a maximum intensity of 0.46 Jy beam^{-1}, implying that it had a compact structure. Interestingly, on 2009 April 11–12, as shown in figure 2, the $v = 3$ emission suddenly increased by a factor of $\sim$25, comparable to that reported in Cho et al. (1996), and was detected in all baselines including the VERA Mizusawa telescope.

Taking into account results of the monitoring observations of stellar H_2O masers (Shintani et al. 2008), a flux maximum of H_2O maser emission in W Hya, with a light curve period of 361 d, was expected around the beginning of 2009 January, 3–4 months after the optical maximum. Pardo et al. (2004) predicted that the SiO flux maximum in W Hya may occur a few weeks after the optical maximum. Therefore, it is expected that the present SiO maser observations were made 4–5 months after the SiO maser flux maximum, or just before the flux minimum. In fact, the flux densities of the $v = 1$ and $v = 2$ lines dropped during 2009 February–April. A flux decline of the $v = 1$ and $v = 2$ lines was also found from February 27 to 28 (figure 1b). Therefore, as mentioned above, the increase in the $v = 3$ flux density is a unique phenomenon.

We compare the $v = 1$ and $v = 2$ maser distributions observed on February 27 and between the $v = 2$ and $v = 3$ maser distributions on February 28. In order to compare the $v = 1$, 2, and 3 maser distributions, first we compare the $v = 2$ distributions observed on February 27 and 28. Figure 1b shows the spectra of the $v = 2$ emission observed on the two days. A systematic decrease in the flux density scale in the whole spectrum is observed. For the JVN data in which the system noise temperatures were measured in all stations, an error of the flux scale calibration was estimated to be $\lesssim 10\%$. By considering the dramatic decline in the $v = 1$ and $v = 2$ flux densities during 2009 February–April, as mentioned above, this indicates an intrinsic variation in the maser source. At the same time, a temporal variation within the spectrum in some velocity ranges is observed. Figure 3 shows the velocity-integrated brightness distributions of the $v = 2$ emission observed on the two days. A temporal variation in the brightness distribution is clearly recognized. The two maser maps are superposed into a common coordinate frame by using two position-reference maser features, A and B. They were located at $(-28.95, -64.98)/(-0.01, -0.21)$ and $(14.85, 1.64)/(44.16, 66.37)$ [mas] on February 27/28, respectively, in individual coordinate frames. The coordinates of the map on February 28 were shifted by the mean offsets (29.1, 64.7) [mas]. The uncertainty scale of the map superposition among the $v = 1$, 2, and 3 is dominated by the discrepancy in these coordinate shifts of the two position-reference features, $\sigma \sim 0.4$ mas, smaller than the error scale described in equation (1).

Figure 4a shows a composite map of the $v = 1$, 2, and 3 masers observed on February 27 and 28. We find a big difference between similar brightness distributions of the $v = 1$ and 2 maser features and large offsets of the $v = 3$ maser features from those of the former two maser lines. The $v = 3$ maser features were located closer to the central star by $\sim$6 mas. This offset is larger than the uncertainty scale of the map superposition mentioned above, a radius difference ($\lesssim$3 mas), and widths ($\lesssim$4 mas) of the maser feature rings of the $v = 1$ and $v = 2$ lines (figure 4a). The LSR velocities of the $v = 3$ features are closer to the systemic velocity of W Hya ($V_{\rm LSR} \simeq 42\,{\rm km\,s^{-1}}$: Benson et al. 1990). The difference in LSR velocities among the nearest $v = 1$, 2, and 3 maser features are within 2 km s^{-1} (figure 4b). The featured velocity difference of 2 km s^{-1} on the maser clump scale ($\lesssim$10 mas) is still within the typical turbulence velocity amplitude observed in the SiO maser shells, but slightly higher than the thermal velocity width ($\sim 1.5\,{\rm km\,s^{-1}}$) of molecular gas with a stellar surface temperature of $\sim$2600 K.

Figure 5 shows a composite map of the $v = 2$ and $v = 3$ maser emissions observed on April 11 and 12. The two maser maps are superposed onto a common coordinate frame by using position-reference $v = 3$ maser features, C, whose visibilities were used for fringe-fitting and self-calibration. Feature C was located at (64.08, $-$23.37)[mas] in the coordinate frame of the $v = 2$ map. In order to register the $v = 3$ image

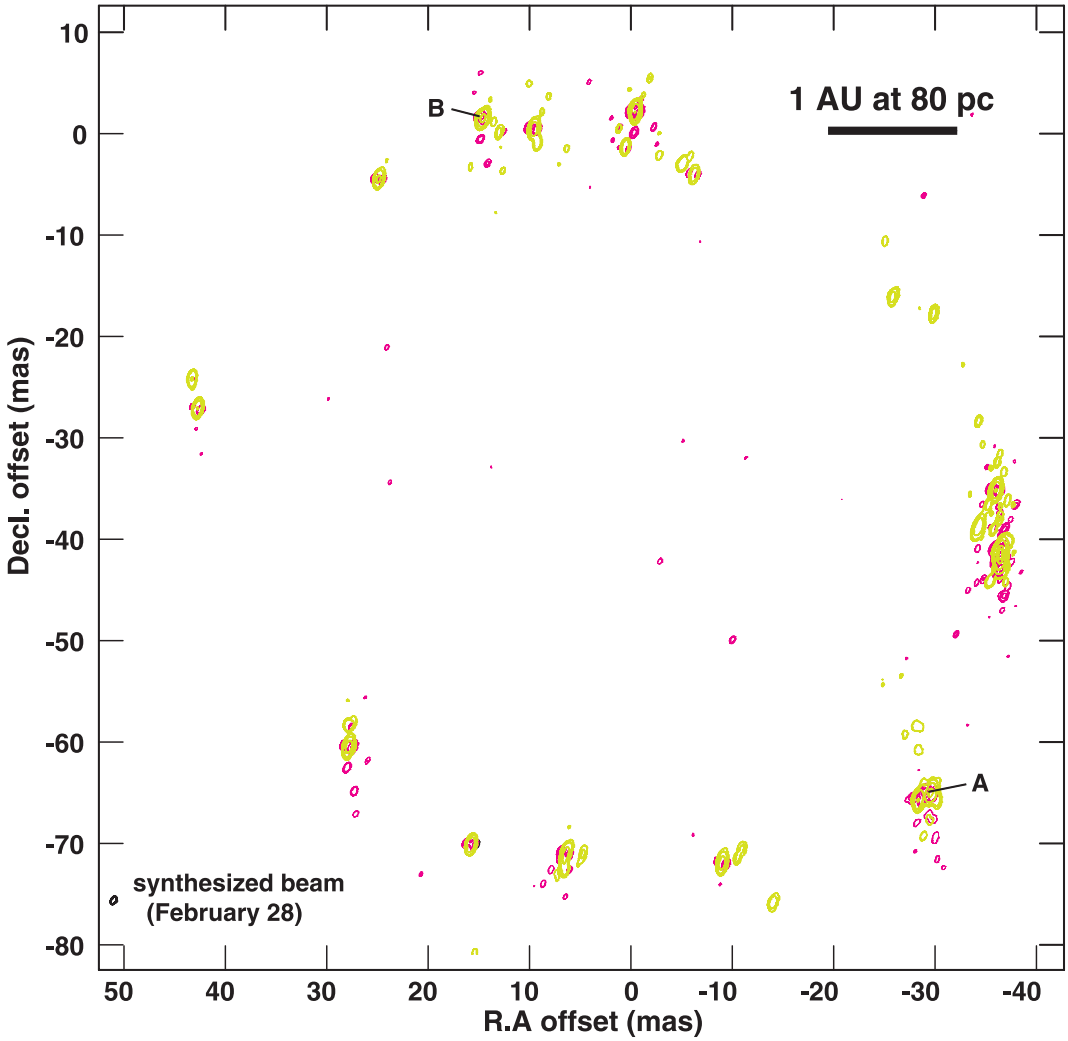

Fig. 3. Comparison between velocity-integrated maps of SiO $v = 2$ $J = 1$–0 maser emission in W Hya observed on February 27 (pink contours) and 28 (yellow-green contours). Contour levels are 0.44, 1.31, 3.94, 11.83, 35.47, and 53.21 Jy beam^{-1} km s^{-1}. Features A and B are used as position references for superposition of the two maps.

obtained in the self-calibration onto the $v = 2$ image, its coordinates were shifted by these offsets. The W Hya SiO masers had a total LSR velocity width of 10 km s^{-1} through all of the present observations; however, no systematic trend in the velocity distribution was found (figures 5b and 5c).

The SiO maser conditions dramatically changed from 2009 February to April. As shown in figure 5a, the number of detected maser features in the $v = 2$ line significantly decreased. On the other hand, the number of detected maser features in the $v = 3$ line increased as their flux densities rose. In addition, the location of the brightest $v = 3$ maser feature was coincident with that of one of the $v = 2$ maser features. The radius of the $v = 3$ maser arc was roughly equal to that of the $v = 2$ maser ring within the uncertainty of the map registration, as typically seen in many SiO maser sources. Note that the brightest parts in the maser ring/arc were quite different between the $v = 2$ (on the west side) and $v = 3$ (on the east side) lines. This is a property of the $v = 3$ line contrasting to the $v = 1$ and $v = 2$ lines, in which their feature locations and brightness distributions have a good correlation, even though there is still a small difference (e.g., Miyoshi et al. 1994). The feature velocity difference of ~ 1 km s^{-1} in the maser clump scale (figures 5b and 5c) is comparable to that found on February 28.

4. Discussion

The present observations show composite VLBI maps of the SiO $v = 1$, 2, and 3 ($J = 1$–0) maser lines for the first time. Notable findings include a dramatic, but not unexpected, decline of $v = 1$ and $v = 2$ SiO ($J = 1$–0) flux densities, a significant decrease in the number of detected $v = 2$ maser features and, in constrast, an increase in the number of detected $v = 3$ maser features as well as an increase in the $v = 3$ flux density. The distribution of the $v = 3$ line also dramatically changed, although they were always more excited on the west side of the entire maser ring.

In VLBI observations of SiO masers in IRC +10011 (O-rich

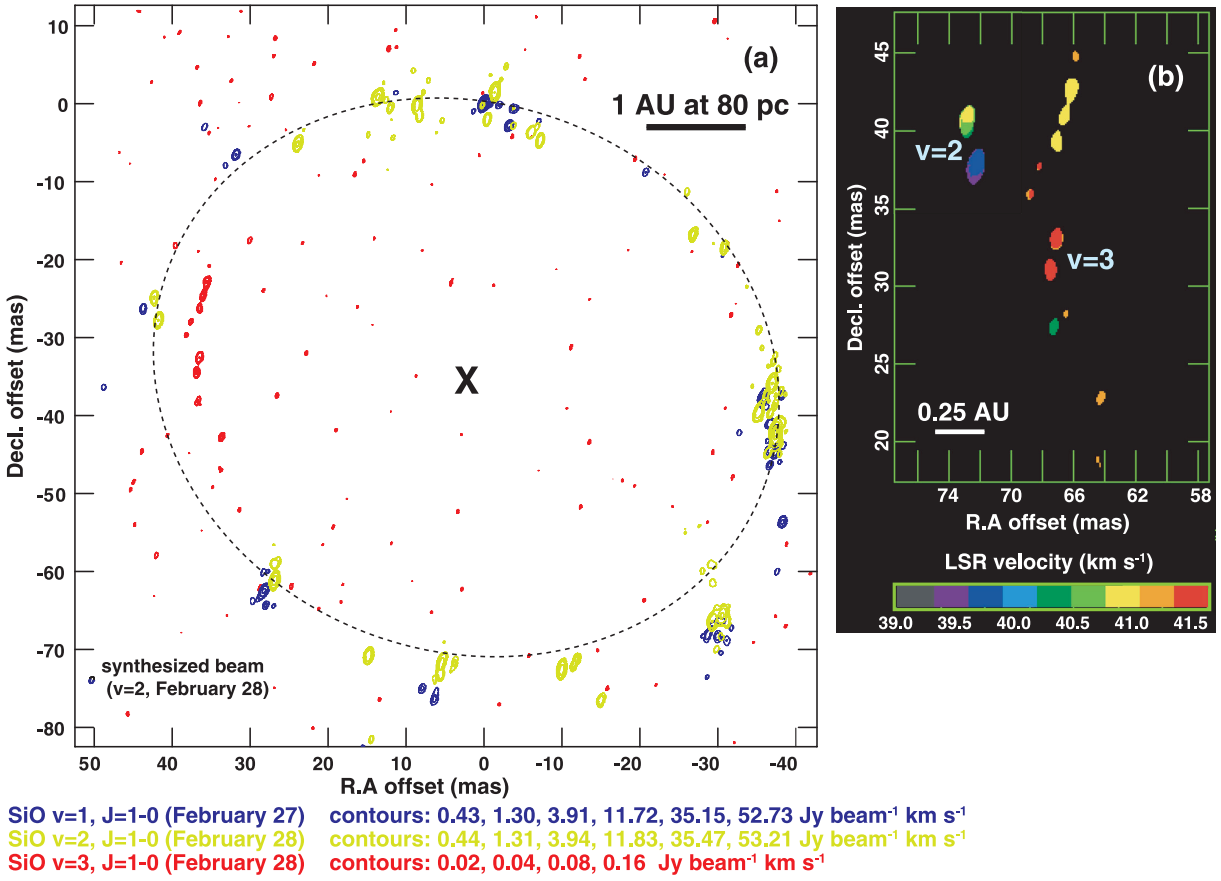

Fig. 4. Comparison among the SiO $v = 1$, 2, and 3 ($J = 1$–0) maser emission observed in W Hya on 2009 February 27–28. (a) Composite velocity-integrated maps of the SiO $v = 1$, 2, and 3 masers. The contour levels are described at the bottom of the figure. The map origin is located at the $v = 2$ maser spot that was observed on February 28 and used as fringe-phase reference. A dashed line ellipse with major and minor axes of 80.0 mas and 71.4 mas, respectively, at a position angle of 70° east from north indicates a ring-shaped brightness morphology of the SiO $v = 1$ and $v = 2$ maser emission roughly fitted by eye. (b) Composite first moment map of the SiO $v = 2$ (eastern two features) and $v = 3$ (other western features) maser emission in W Hya obtained on 2009 February 28. The region showing the $v = 3$ emission is enlarged. The coordinates of the $v = 2$ and $v = 3$ map in figure 4a were shifted by (29.1, 64.7)[mas] from those of the first moment map (see main text about the offset).

Mira) and χ Cyg (S-type Mira), Soria-Ruiz et al. (2004) reported that SiO $J = 2$–1 and $J = 1$–0 masers at $v = 1$ have completely different spatial distributions, while the $J = 1$–0 masers at $v = 1$ and $v = 2$ have similar spatial distributions with slightly different angular distances from the central star. In particular, the spatial coexistence of the $J = 1$–0 lines at $v = 1$ and $v = 2$ as well as quenching of the $J = 2$–1 line at $v = 2$ are significant maser properties. These observational results are well explained by the line-overlap between the ro-vibrational lines ($\nu_2 = 0\ 12_{7,5}$)–($\nu_2 = 1\ 11_{6,6}$) of para-H_2O and ($v = 1\ \ J = 0$)–($v = 2\ \ J = 1$) of SiO (e.g., Langer & Watson 1984). This is the case of O-rich Miras, but not in S-type ones where the $J = 1$–0 line at $v = 2$ is much weaker. Similarly, an enhancement of the $J = 1$–0 line at $v = 3$ and a weakening of the $J = 2$–1 line at $v = 3$ in O-rich Miras have been proposed to be explained by similar line-overlaps in the SiO and H_2O lines (Cho et al. 2007). Note that, these mechanisms require spatial coexistence among the $v = 1$, 2, and 3 lines only with the condition that two overlapped frequencies of the SiO and H_2O lines coincide perfectly within the thermal width. In order to pump from the $v = 2\ \ J = 0$ to the $v = 3\ \ J = 1$ level, a mid-IR radiation with a wavelength almost equal to that for pumping from the $v = 1\ \ J = 0$ level to the $v = 2\ \ J = 1$ level is necessary. Since these pumping transitions should occur at the same location, a spatial coincidence between the $J = 1$–0 lines at $v = 2$ and $v = 3$ is also required. However, the difference in frequencies and in optical depths of these IR pumping lines may create offsets of the maser distributions. A more careful investigation of the LSR velocity differences and theoretical models for calculating the IR opacities in the circumstellar envelopes could be used to judge this issue. In this case, the velocity field in the CSE should also be taken into account. If a simultaneous excitation of the three maser lines occurs by a fine tuning of the Doppler frequencies of the transitions, then spatial offsets should have different characteristics between the CSE velocity fields dominated by systematic deceleration/acceleration and turbulence motions.

For the case of the SiO $v = 1$ and $v = 2$ masers in the O-rich star W Hya, the maser distributions are roughly consistent with those reported in Soria-Ruiz et al. (2004). For the case of the $v = 3$ line, however, the proposed line-overlap mechanism cannot explain the positional difference between the $v = 3$ and

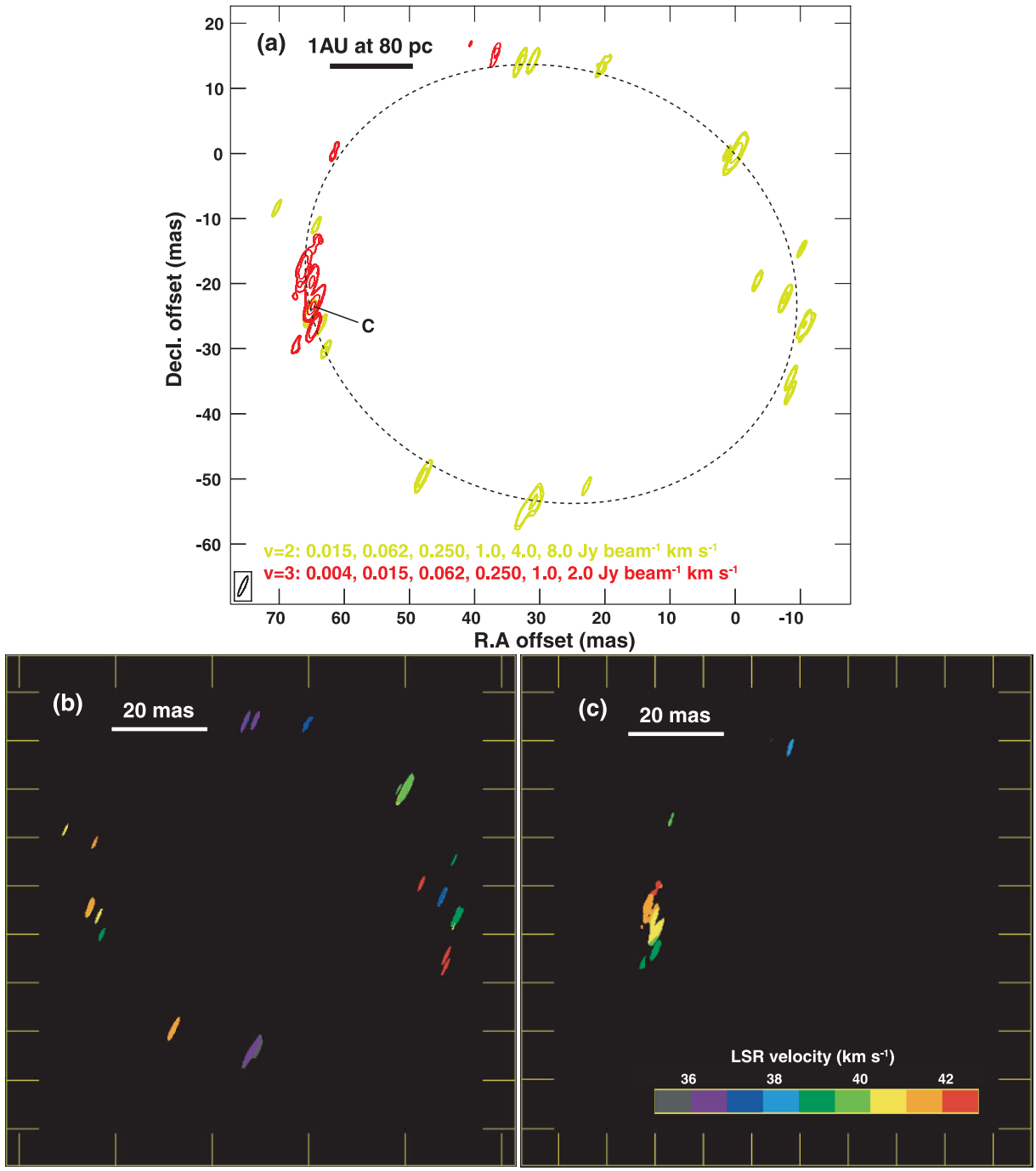

Fig. 5. Comparison between the maps of SiO $v = 2$ and $v = 3$ ($J = 1$–0) maser emissions observed in W Hya on 2009 April 11–12. (a) Contour maps of the SiO $v = 3$ (red) and $v = 2$ (yellow-green) emissions. SiO $v = 3$ maser feature C was used as position references for exchanging from the $v = 3$ map synthesized on the basis of the phase-referencing technique with the $v = 2$ emission data to that on the basis of the self-calibration technique. A dashed-line ellipse with major and minor axes of 75.2 mas and 67.1 mas, respectively, at a position angle of 70° east from north indicates a ring-shaped brightness morphology of the SiO $v = 2$ and $v = 3$ maser emissions roughly fitted by eye. (b) First moment map of the SiO $v = 2$ emission. (c) Same as (b) but for the SiO $v = 3$ emission. The local-standard-of-rest velocity of the SiO maser emission in (b) and (c) is indicated in a horizontal color bar.

$v = 2$ masers observed on 2009 February 27–28. As an alternative model, the collisional pumping model (Lockett & Elitzur 1992) is proposed. It suggests that the $J = 1$–0 line at $v = 3$ cannot be excited at the location where the spatial coexistence of the $J = 1$–0 lines at $v = 1$ and $v = 2$ was found. Instead, the former line should be excited in the inner part of the CSE. Even though at lower vibrational levels the line overlap mechanism may be predominant, at higher vibrational levels the collisional pumping mechanism may become the major one. However, collisional pumping will require a non-local thermodynamical equilibrium (non-LTE) condition in the CSE such as the propagation of shock waves enhanced by stellar pulsation. The

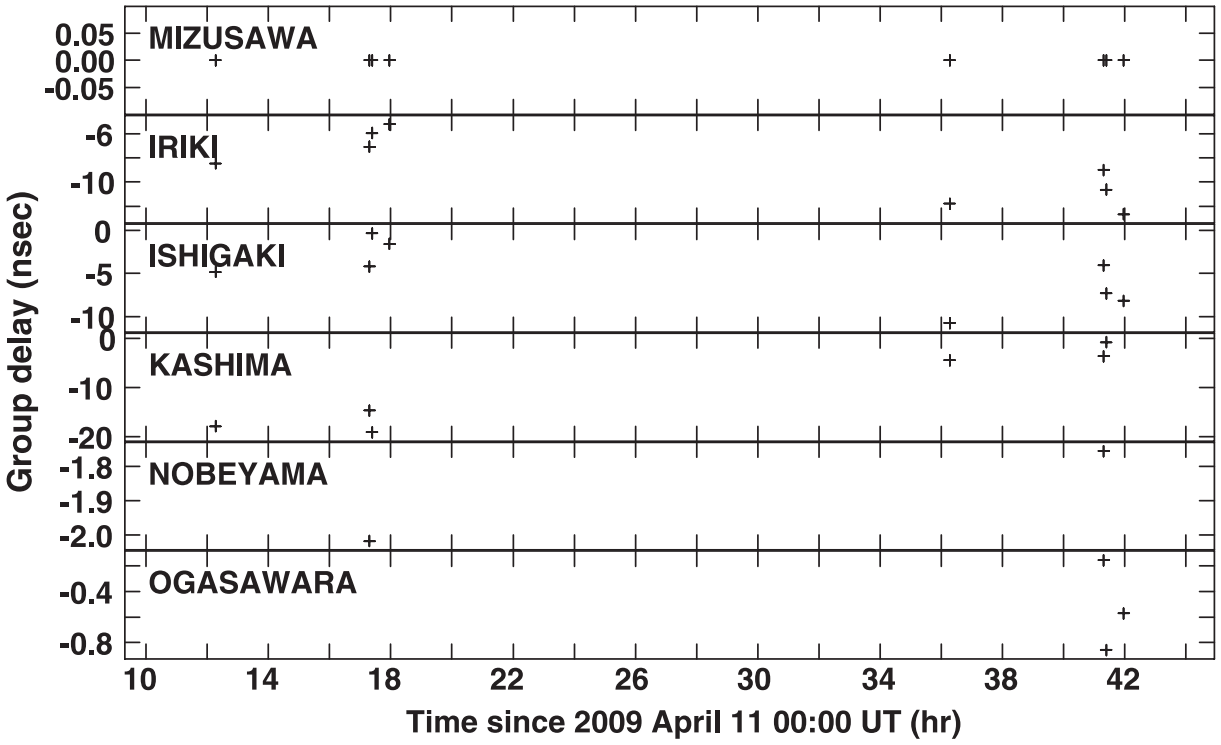

Fig. 6. Fringe-fitting solutions obtained from scans of 3C 273, ICRF J162546.9−252738, and NRAO 530 in the session r09101a–r09102a. The VERA Mizusawa station was the reference antenna in the fringe fitting.

observed temporal variations of the $v = 2$ and $v = 3$ lines seem to be inconsistent with the direction of the outward shock propagation, in which the temporal variation in the spatial distribution and flux density of the $v = 3$ masers shoud be followed by those of the $v = 2$ masers. An alternative reason for this inconsistency is the inhomogeneity of the CSE. It is worthwhile to mention that Reid and Menten (2007) find a radio photosphere of W Hya that is elongated in the east–west direction, at which bright SiO maser features, as shown in the present paper, are excited. Taking into account the quick variation of the $v = 3$ maser distribution within 40 days, the mechanism of *predominant pumping* should be considered, which is always working for any SiO maser excitation with a smaller correlation with the stellar pulsation.

In the present VLBI observations, the registration of the $v = 1$, 2, and 3 lines is imperfect and introduces a registration uncertainty of ~ 2.3 mas. However, the current VLBI technology including digital sampling, signal recording, and data correlation already enables us to simultaneously observe all of the three maser lines as well as other SiO maser transitions whose frequencies are included within a frequency width of 1 GHz. If astrometric observations made with VERA are conducted with the above-mentioned multi-frequency observations, the maser distributions can be directly mapped onto a common reference frame with respect to extragalactic position reference sources, such as quasars. Multi-epoch systematic VLBI observations spanning a whole stellar pulsation period as made with the VLBA (Diamond & Kemball 2003) should be performed in order to trace the temporal variation in the SiO maser pumping conditions for unambiguously elucidating the physical evolution of the CSE.

5. Conclusions

The first VLBI detection of SiO $v = 3$ $J = 1$–0 in the present paper should shed new light on understanding the excitation mechanism of SiO maser emission around evolved stars. In contrast to the $v = 1$ and $v = 2$ masers, which have similar distributions, and are suggested to be excited by the line-overlap mechanism, it seems that the $v = 3$ masers may be located closer to the central star than the $v = 1$ and $v = 2$ masers, and may be excited by a collisional pumping mechanism at that time. However, the line-overlap mechanism is still expected to be a possible mechanism to excite exceptionally bright $v = 3$ maser emissions. Long-term systematic observations of multi-transitions of SiO masers in VLBI astrometric mode with new VLBI backend systems should directly provide important clues to unambiguously identify major maser pumping schemes.

We acknowledge all staff members and students who have helped in array operation and in data correlation of the JVN/VERA. We also thank Bosco Yung and Sze Ning Chong for careful corrections of the manuscript. We also appreciate Dr. Phil Diamond for providing critical comments on the data-analysis procedures. HI and SD have been financially supported by a Grant-in-Aid for Scientific Research from Japan Society for Promotion Science (20540234). JN was supported

by the Research Grants Council of the Hong Kong under grants HKU703308P and HKU704209P, and by the financial support from the Seed Funding Programme for Basic Research in HKU (200802159006).

Appendix. Accuracy of Group-Delay Determination over the 300 MHz Bandwidth

A position error, σ_θ, of a maser spot detected at a frequency of $\nu = \nu_{\rm ref} + \Delta\nu$ contributed from a group-delay residual uncertainty, $\sigma_{\tau_{\rm g}}$, is evaluated from the following equation for the present observations:

$$\sigma_\theta \approx \frac{\Delta\nu}{\nu}\frac{c}{D}\sigma_{\tau_{\rm g}} \simeq 0.43(\sigma_{\tau_{\rm g}}[{\rm ns}])\ \ [{\rm mas}], \tag{A1}$$

where $\nu_{\rm ref} \simeq 42.8$ GHz is the frequency of the spectral channel used in the visibility calibration and D the VLBI baseline (typically $D \simeq 1000$ km in the present observations).

We estimated the group-delay calibration error to be within $\sigma_{\tau_{\rm g}} < 5$ ns in a single observation session as follows. We observed a calibrator, ICRF J134215.3−290041, 1.°6 away from W Hya, every 30 min, but it could not be detected. Instead, we used the data of 3C 273, ICRF J162546.9−252738, and NRAO 530 for group-delay measurements, but these calibrators have much larger angular distances from W Hya, leading to additional delay residuals, and were observed at only the beginning and end of the whole observation session. Figure 6 shows the results of group-delay measurements in r09101a–r09102a. The group-delay solutions were scattered within 5 ns on a time scale of 6 hours among the different calibrators far away from W Hya. Note that the individual solutions should have an uncertainty smaller than 0.5 ns, which is calculated from the thermal-noise contribution. They also changed by up to 20 ns in two days (in the Kashima station), but can be interpolated in the maser data calibration. We are convinced this because we have confirmed that the clock offsets, a major contribution to the delay residual, have been stable to within 5 ns in each of previous JVN observation. Thus, we adopt an upper limit of 2.2 mas to the contribution of such a group-delay factor to the uncertainty scale of the maser map superposition among $v = 1$, 2, and 3.

References

Benson, P. J., et al. 1990, ApJS, 74, 911
Cho, S.-H., Kaifu, N., & Ukita, N. 1996, A&AS, 115, 117
Cho, S.-H., Lee, C. W., & Park, Y.-S. 2007, ApJ, 657, 482
Desmurs, J. F., Bujarrabal, V., Colomer, F., & Alcolea, J. 2000, A&A, 360, 189
Diamond, P. J., & Kemball, A. J. 2003, ApJ, 599, 1372
Humphreys, E. M. L., Gray, M. D., Yates, J. A., Field, D., Brown, G. H., & Diamond, P. J. 2002, A&A, 386, 256
Knapp, G. R., Pourbaix, D., Platais, I., & Jorissen, A. 2003, A&A, 403, 993
Langer, S. H., & Watson, W. D. 1984, ApJ, 284, 751
Lockett, P., & Elitzur, M. 1992, ApJ, 399, 704
Matsumoto, N., et al. 2008, PASJ, 60, 1039
Miyoshi, M., Matsumoto, K., Kameno, S., Takaba, H., & Iwata, T. 1994, Nature, 371, 395
Nakashima, J., & Deguchi, S. 2007, ApJ, 669, 446
Pardo, R. R., Alcolea, J., Bujarrabal, V., Colomer, F., del Romero, A., & de Vicente, P. 2004, A&A, 424, 145
Reid, M. J., & Menten, K. M. 2007, ApJ, 671, 2068
Shintani, M., et al. 2008, PASJ, 60, 1077
Soria-Ruiz, R., Alcolea, J., Colomer, F., Bujarrabal, V., Desmurs, J.-F., Marvel, K. B., & Diamond, P. J. 2004, A&A, 426, 131
Vlemmings, W. H. T., van Langevelde, H. J., Diamond, P. J., Habing, H. J., & Schilizzi, R. T. 2003, A&A, 407, 213
Yi, J., Booth, R. S., Conway, J. E., & Diamond, P. J. 2005, A&A, 432, 531